Title

Dairy Methane Emissions in California's San Joaquin Valley Inferred With Ground-Based Remote Sensing Observations in the Summer and Winter

Journal

Journal of Geophysical Research: Atmospheres, 126(24)

ISSN

2169-897X

Authors

Heerah, Sajjan
Frausto-Vicencio, Isis
Jeong, Seongeun
et al.

Publication Date

2021-12-27

DOI

10.1029/2021jd034785

Peer reviewed

JGR Atmospheres

RESEARCH ARTICLE
10.1029/2021JD034785

Special Section:
Carbon Weather: Toward the next generation of regional greenhouse gas inversion systems

Dairy Methane Emissions in California's San Joaquin Valley Inferred With Ground-Based Remote Sensing Observations in the Summer and Winter

Sajjan Heerah[1], Isis Frausto-Vicencio[2], Seongeun Jeong[3], Alison R. Marklein[2], Yifan Ding[4], Aaron G. Meyer[1], Harrison A. Parker[5], Marc L. Fischer[3], Jonathan E. Franklin[6], Francesca M. Hopkins[2], and Manvendra Dubey[1]

[1]Earth and Environmental Sciences, Los Alamos National Laboratory, Santa Fe, NM, USA, [2]Department of Environmental Sciences, University of California Riverside, Riverside, CA, USA, [3]Energy Technologies Area, Lawrence Berkeley National Laboratory, Berkeley, CA, USA, [4]Department of Mechanical Engineering, University of California Riverside, Riverside, CA, USA, [5]Division of Geological and Planetary Sciences, California Institute of Technology, Pasadena, CA, USA, [6]School of Engineering and Applied Sciences, Harvard University, Cambridge, CA, USA

Abstract The dairy industry in the San Joaquin Valley (SJV) is one of California's largest methane (CH_4) sources. Reducing dairy emissions is a priority for the state's climate change plans. Observations of current dairy CH_4 emissions are key to monitoring actions taken toward this goal. To help support this, we present new ground-based measurements of atmospheric column-averaged CH_4 mixing ratio (XCH_4) gradients across a group of 600 dairies in the central SJV using EM27/SUN solar spectrometers. We used measurements from the 2019 summer and 2020 winter seasons for a top-down emission inversion based on the WRF-STILT model. Our top-down estimates of the region's dairy emissions range from 90% to 183% of the current CALGEM inventory's emissions of 277 Gg/yr. In contrast to the strong temperature dependence found by earlier dairy CH_4 emission studies, we also find that our top-down emissions during the winter measurement days are comparable to the summer measurement days, possibly due to seasonal changes in dairy management practices and meteorological conditions. Furthermore, we find significant interday variability in our measurements and find that our emission estimates overlap with earlier top-down studies and bottom-up inventories in this region. Our study demonstrates how analysis of ground-based remotely sensed CH_4 gradient observations can help improve our understanding of CH_4 sources at scales relevant to mitigation policy. It also reflects the need for long-term monitoring of CH_4 emissions in the region and at individual facilities to better understand their emissions.

Key Points:

- We present total column measurements of the San Joaquin Valley's dairy methane emissions using EM27/SUN spectrometers over 6 measurement days
- Top-down emission estimates from this data show interday variability and overlap with published San Joaquin Valley emission estimates
- Our measurements' winter emissions are comparable to summer emissions in contrast to patterns expected due to temperature

Supporting Information:

Supporting Information may be found in the online version of this article.

Correspondence to:

S. Heerah and M. Dubey,
sajjanh2@gmail.com;
dubey@lanl.gov

Citation:

Heerah, S., Frausto-Vicencio, I., Jeong, S., Marklein, A. R., Ding, Y., Meyer, A. G., et al. (2021). Dairy methane emissions in California's San Joaquin Valley inferred with ground-based remote sensing observations in the summer and winter. *Journal of Geophysical Research: Atmospheres*, *126*, e2021JD034785. https://doi.org/10.1029/2021JD034785

Received 19 FEB 2021
Accepted 31 OCT 2021

1. Introduction

Global concentrations of atmospheric CH_4 have substantially increased since 1750 due to the expansion of human agriculture, waste management, and fossil fuel usage (Dlugokencky et al., 2011). CH_4 is a 28 times stronger greenhouse gas than carbon dioxide (CO_2) on a century timescale and increased atmospheric CH_4 accounts for 25% of anthropogenic climate forcing to date (Etminan et al., 2016). CH_4 has also contributed to increases in tropospheric ozone, an air pollutant and short-lived greenhouse gas (Fiore et al., 2008), and to stratospheric water vapor, which acts as a sink for stratospheric ozone (Myhre et al., 2013). Additionally, CH_4 has an atmospheric lifetime of 9.8 years, so its atmospheric abundance quickly responds to changes in its emissions (Saunois et al., 2016). Furthermore, there are proven and cost-effective ways to reduce emissions (UNEP, 2011). These characteristics make reducing CH_4 emissions an attractive policy option for mitigating the effects of climate change in the near and intermediate term.

The US state of California is committed to reducing its CH_4 emissions to 40% of 2013 levels by 2030 as part of its climate change policy (CARB, 2017). The state has funded specific policies to reduce its emissions, including from its large dairy sector, which makes up 19% of the United States's milk production (CDFA, 2020). CH_4 emissions from the dairy sector are from two main sources: enteric fermentation emissions produced by dairy cows' digestion process and manure management emissions created by the anaerobic decomposition of dairy waste. Emissions from the dairy sector are estimated by the state as 880 Gg/yr, accounting for about half of California's total CH_4 emissions (CARB, 2019). The dairy industry is centered in the San Joaquin Valley (SJV), which contains 87% of the state's 1.7 million large dairy herd (CDFA, 2020). The SJV has also been identified as a large North American CH_4 emissions hotspot in many studies, highlighting the global importance of the region's dairy

CH_4 emissions (Kort et al., 2014; Turner et al., 2015; Wecht, Jacob, Frankenberg, et al., 2014; Zhang et al., 2020). Dairies in the SJV are also intensively managed and offer opportunities for large emission reductions, such as by installing digesters to capture manure emissions.

Despite the magnitude of dairy CH_4 emissions, different methodologies for estimating emissions disagree on their size and little is known about their variability in time and space. Bottom-up methods use process-based emission factors with data on CH_4 emitting activities in a region to estimate emissions. Uncertainty is introduced in these methods by uncertainties in the emission factors and activity data used to calculate them, particularly at regional scales (Marklein et al., 2020). California currently uses bottom-up methods to track its total emissions (CARB, 2019). In contrast, top-down approaches are based on measurements of atmospheric CH_4 and modeling the transport of CH_4 emissions in the atmosphere. In California, several top-down studies have found that bottom-up CH_4 inventories may underestimate emissions from the statewide dairy sector and in the SJV region specifically (Cui et al., 2017; Jeong et al., 2016; Miller et al., 2013; Trousdell et al., 2016; Turner et al., 2015; Wecht, Jacob, Sulprizio, et al., 2014). This discrepancy has important implications for developing baseline estimates against which the state's emission reduction policies are bench-marked, underscoring the need for research to improve our understanding of the dairy sector's emissions as a function of season and management practices.

Dairy CH_4 emissions are also thought to be seasonally variable. Temperature is known to act as a strong control of emissions from dairy farms' manure systems because of its effect on microbial productivity (Arndt et al., 2018; Husted, 1994). This is the only seasonal effect that is included in the US-wide bottom-up inventory of monthly dairy emissions created by Maasakkers et al. (2016), which is presently the only published US-wide, sub-annual CH_4 inventory. However, there is evidence that other factors could significantly contribute to seasonality in dairy CH_4 emissions. During periods of high soil moisture, dairy cows are kept inside longer, which increases the amount of waste entering liquid manure systems where it can be converted to CH_4 (Meyer et al., 2019). The size of this effect is uncertain as it depends on the management choices at individual dairies as well as precipitation. Previous studies have also found that the build-up of waste in liquid waste systems during unfavorable CH_4 production conditions and management choices on individual dairy farms can dramatically impact their emissions (Leytem et al., 2017; VanderZaag et al., 2014). Other factors that cause agitation of the liquid waste systems such as wind, rainfall, or mechanical pumping have also been found to impact individual dairy farms' emissions (Leytem et al., 2017). Studies attempting to quantify the amplitude of the seasonal variability of SJV dairy emissions are limited and have shown conflicting results. Jeong et al. (2016) did not find significant seasonality in the statewide dairy source using ground-based in-situ measurements while Arndt et al. (2018) reported that emissions at two Californian dairy farms were lower in the winter than in the summer due to a temperature effect. Seasonality in the region, therefore, remains an important gap in our understanding of dairy methane emissions.

Atmospheric CH_4 enhancements from a region of interest can be measured by remote sensing. Ground or satellite based remote sensing instruments can use the absorption of sunlight through the atmosphere by a particular gas to derive its average mixing ratio over the entire atmospheric column (Xgas). Xgas measurements are less sensitive to errors in difficult-to-model phenomena such as small-scale turbulence and vertical mixing compared to in-situ measurements taken in the atmospheric boundary layer (McKain et al., 2012). Because they measure the entire atmospheric column, they are also more sensitive to fluxes at regional scales compared to in-situ measurement techniques (Keppel-Aleks et al., 2011; Lauvaux & Davis, 2014). Several studies have demonstrated the usefulness of both ground and satellite-based Xgas measurements to provide top-down estimates of emissions at regional scales (km to 10s of km scales) such as urban regions (Hase et al., 2015; Hedelius et al., 2018; Jones et al., 2021; Makarova et al., 2021; Schwandner et al., 2017; Vogel et al., 2019; Wu et al., 2018, 2020; Wunch et al., 2009, 2019; Ye et al., 2020; Zhao et al., 2019), fossil fuel-producing basins (Kort et al., 2014; Luther et al., 2019; Zhang et al., 2020), agricultural regions (Chen et al., 2016; Kille et al., 2019; Viatte et al., 2017) and in state and country-level domains (Shekhar et al., 2020; Turner et al., 2015; Wecht, Jacob, Frankenberg, et al., 2014). This makes Xgas measurements a good complement to other previously used techniques like aircraft and tower-based in-situ measurements for inferring dairy CH_4 emissions in the SJV. To date, however, ground-based remote sensing measurements have not been used to measure CH_4 emissions in the SJV.

Our study aimed to measure emissions from a large grouping of dairies in the central part of the SJV (about 600 dairy farms over approximately 9×10^3 km^2) using a network of ground-based remote sensing instruments, the EM27/SUN, during three field measurement periods in the region (July 2019, September 2019, and January–February 2020). Emissions in this part of the SJV are weakly constrained by past measurements and measuring them

is considered a priority for understanding California's emissions because of the high concentration of agricultural sources in the area (Cui et al., 2019). We used these EM27/SUN measurements with the Lagrangian atmospheric transport model, STILT (Fasoli et al., 2018), to create top-down estimates of emissions in the region. We used these estimates to assess variability in the SJV's dairy CH_4 emissions during our measurement days and compared them to published bottom-up and top-down estimates of emissions in the region. This analysis gives new independent constraints on CH_4 emissions in the SJV and demonstrates how ground-based remote sensing data can be used to infer regional greenhouse gas emissions.

2. Materials and Methods

2.1. Central San Joaquin Valley Study Area

We made our measurements in the SJV, illustrated in Figure 1. The SJV is a flat region bounded by mountains on its eastern, western, and southern sides. In the north, the SJV merges with the Sacramento Valley. Air typically enters the SJV from the northwest near the San Joaquin Delta and remains confined in the SJV for long periods (San Joaquin Valley United Air Quality District, 2004). This containment mixes and traps air pollutants and greenhouse gases in the SJV.

As an a-priori map of emissions in the area, we used the non-dairy emission inventory from CALGEM (Fischer, 2017; Jeong et al., 2016) along with a new dairy CH_4 inventory (Marklein et al., 2020). CALGEM is a high resolution (0.1°) disaggregation of California's regulatory CH_4 inventory that uses detailed spatial information to distribute emissions from the regulatory inventory. Its total emissions are scaled to match the regulatory inventory' total statewide CH_4 emissions. For the dairy sector, we used a facility level inventory of annual dairy emissions created by Marklein et al. (2020) gridded at a 0.1° resolution. Their inventory draws on farm level permitting information and regionally specific manure management practices to estimate and localize dairy emissions at a higher accuracy than CALGEM's dairy inventory.

Our EM27/SUN measurements were focused on capturing emissions from a large grouping of dairies in Tulare and Kings counties in the central part of the SJV. In the a-priori inventory used in this study, these counties emit 362 Gg CH_4/year with most emissions (89%) from the dairy sector. The next largest CH_4 source in this region is natural gas transmission and distribution emissions concentrated in urban areas. South of the area, in Kern County, there is also significant oil and natural gas extraction and processing related CH_4 emissions, but these sources are typically downwind and unsensed by our instruments.

On all measurement days, one instrument was located to the northwest of the dairy grouping at Cantua Creek (36.445°N, −120.248°E, 86 m above sea level (a.s.l.)) and one instrument was located to the southeast of the diaries at Terra Bella (35.931°N, −119.036°E,153 m a.s.l.). Prevailing winds in the SJV are from the northwest so these instruments typically captured background air upwind of the dairies and polluted air downwind of them. On measurement days when we had three instruments, the third instrument was located at either a site south of the dairy grouping at Helm's Corner (36.084°N, −119.644°E, 53 m a.s.l.) or at a site to the east of the dairies at Visalia (36.308°N, −119.194°E, 110 m a.s.l.). The specific location of the third instrument site was determined by the forecast winds on each measurement day. The distance between the instruments was on the order of 10s of kilometers which was similar to the size of the Xgas measurement networks used in Hedelius et al. (2018) and Vogel et al. (2019).

2.2. EM27/SUN XCH_4 Measurements

The EM27/SUN is a compact field deployable solar tracking Fourier transform spectrometer further described in Gisi et al. (2012). The instrument uses direct solar absorption spectroscopy to retrieve total column abundances of CH_4, CO_2, CO, H_2O, and O_2 along an atmospheric path from the instrument to the sun over a 9–11 s measurement period. The abundances are converted to dry air mixing ratios by dividing by the retrieved oxygen column and using the known column average concentration of O_2. The EM27's XCH_4 measurements have a precision of 0.06% at a 10 min integration time and can be reliably tied to the World Meteorological Organization (WMO) trace gas scale (Chen et al., 2016; Hase et al., 2015; Hedelius et al., 2016).

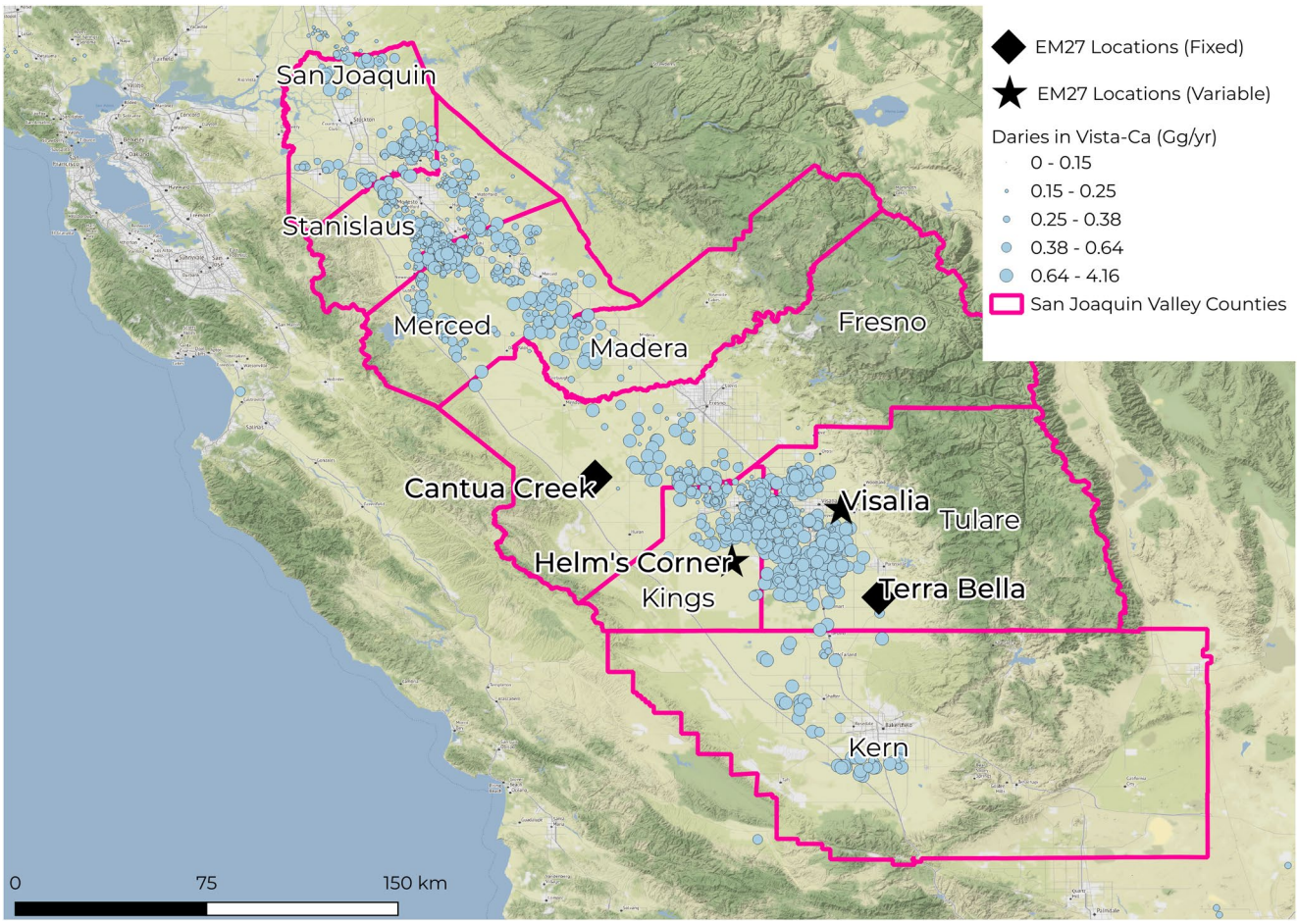

Figure 1. Map of the study area in the San Joaquin Valley. The Valley's counties are outlined in pink. EM27/SUN measurement locations are shown as black symbols and dairy facilities in the region are shown as blue circles, sized by their total emissions in the dairy CH_4 inventory by Marklein et al. (2020). Map tiles by Stamen Design, under CC BY 3.0 and data by OpenStreetMap, under CC BY SA.

We deployed three EM27's owned by Los Alamos National Lab (LANL), NASA's Jet Propulsion Lab (JPL) and Harvard University to the SJV for 2 days during the 2019 summer (July 22 and September 12) and for 4 days in the 2020 winter (January 22, 27, 30, and February 3). The LANL and JPL instruments were used during both seasons and the Harvard instrument was used only in the winter. The LANL and JPL instruments were co-located with Zeno weather stations and the Harvard instrument was co-located with a Digital Instruments MHB-382SD weather station. These stations were used to provide accurate surface pressure values for the EM27 retrievals. Additionally, we used temperature, pressure and humidity profiles from the NCEP/NCAR reanalysis product (available at https://psl.noaa.gov/data/gridded/data.ncep.reanalysis.html) interpolated to each measurement station for the retrievals. This was done instead of using a common meteorological profile because of the large distance between the sites, following Hedelius et al. (2016).

XCH_4 measurements were retrieved from unaveraged double-sided interferograms using the GGG and i2s software distributions (Wunch et al., 2015) and the EGI tool suite (Hedelius & Wennberg, 2019). We used the absorption windows described by Hedelius et al. (2016) for our retrievals. Within 1–2 weeks of our field measurements, we calibrated our instruments by making measurements with the EM27/SUN's at the NASA Armstrong Total Carbon Column Observing Network (TCCON) site (July campaign) or the Californian Institute of Technology TCCON site (September 2019 and January 2020). The TCCON is a network of high resolution solar Fourier transform spectrometers which are tied to the WMO trace gas scale using aircraft measurements of vertical concentration profiles (data available at https://tccondata.org/). We calculated multiplicative offsets for the EM27 XCH_4 retrieval relative to the TCCON observations following the methodology outlined by Hedelius et al. (2016), tying our retrievals to

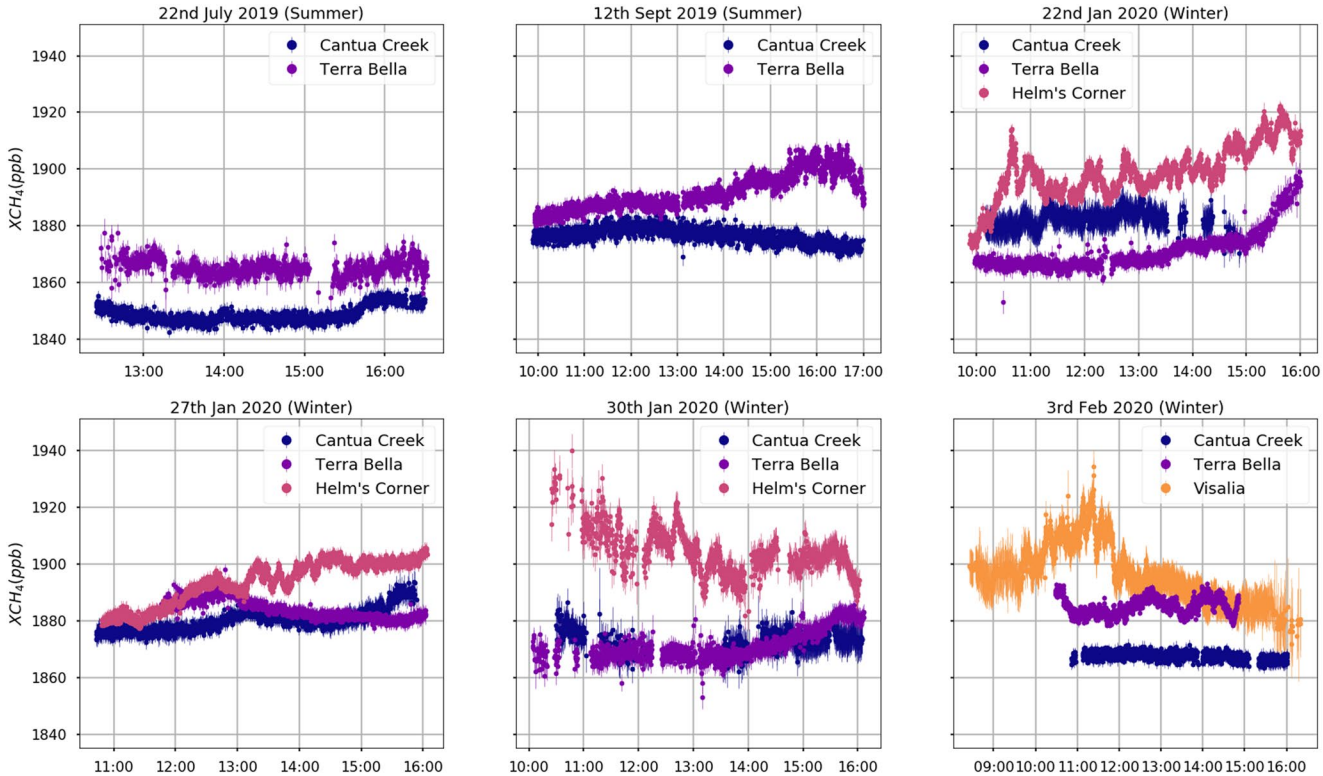

Figure 2. Plots showing unaveraged 11 s resolution XCH_4 measurements from each EM27/SUN on the measurement days. Offsets to the TCCON are applied to the measurements. The error bars represent the 1 sigma precision of the XCH_4 retrievals calculated by GGG.

the WMO scale. This calibration also ensured that any systematic offsets between the EM27/SUN's were removed, allowing for accurate measurements of XCH_4 gradients for our top-down inversions. The correlation plots between the EM27's and the TCCON are shown in Figure S1 in Supporting Information S1. The XCH_4 measurements collected by the EM27/SUN's on all the measurement days are shown in Figure 2.

2.3. STILT: Modeling Emissions Transport

To simulate the atmospheric transport of emissions to our instruments, we used a modified version of the Stochastic Time Inverted Lagrangian Transport model (STILT; Fasoli et al., 2018; Lin, 2003). STILT uses a 4D meteorological field to calculate back trajectories from a receptor location and then analyzes these trajectories to determine a sensitivity footprint. This footprint represents how sensitive a measurement at the receptor is to emissions from different areas and times. The modified STILT version models the Xgas measurements made by the EM27/SUN by creating a slant profile of receptors oriented from the instrument location to the sun (Jones et al., 2021). This creates a profile of emission sensitivity footprints along the measurement columns of the EM27s, $F(z, t)$, representing the sensitivity of CH_4 mixing ratios at different heights to surface emissions, E. Convolving $F(z, t)$ and E create a mixing ratio enhancement profile reflecting the effect of surface emission along the slant EM27 measurement profile at the measurement location and time.

We ran STILT using meteorological fields generated using the WRF model (V 3.9.1) (Skamarock et al., 2008). These fields were run in a nested 36, 12, and 4 km resolution domain centered over western North America with 50 vertical levels from the surface to a pressure height of 100 mb. Boundary conditions for the WRF fields came from the North American Regional Reanalysis forecast product. The model was configured with the MYNN boundary layer parametrization and other options were based on previous work by Jeong et al. (2016) and Bagley et al. (2017) using WRF in the SJV. We used only the MYNN model rather than changing boundary layer para-

metrization in the winter as done in these other studies because we found that the MYNN model showed a better fit with our XCH_4 measurements (Text S3 in Supporting Information S1).

STILT was run using the vertical profile spacing (100 m spacing in the first 3 km of the atmosphere and 500 m spacing above 6 km) and particle release numbers (200 at each vertical level) suggested by Wu et al. (2018) for modeling Xgas signals. For other model control parameters, we used the default STILT parameters described by Lin (2003) and Fasoli et al. (2018). We also ran STILT backwards in time for 7 days as we found that this was sufficient time for the particles to leave the SJV, ensuring that we captured the full influence of the region's emissions.

2.4. Calculating Background CH_4

Aside from the influence of emissions, XCH_4 measurements can vary due to differences in the influence of the far-field CH_4 mixing ratios and differences in the atmospheric column caused by elevation differences (Hedelius et al., 2017). Neglecting these effects can introduce spurious XCH_4 gradients which propagate into emission estimates derived with these measurements.

We generated a background XCH_4 time series for each of our instruments to account for these effects. We did this using the Copernicus Atmosphere Monitoring Service near realtime model (CAMS-NRT) model which provides forecast fields for greenhouse gas mixing ratios and atmospheric variables at a 6-hr and 0.4° grid (Inness et al., 2019). In the first 6 km of the slant model profile, we followed STILT back trajectories from our measurement locations at each measurement time to their endpoints after 7 days. These endpoints were typically over the Pacific. The CAMS model was interpolated to these endpoints to set a dry air CH_4 mixing ratio for each back trajectory. The average of these concentrations was taken as the background concentration for a specific height in the model profile for each measurement location and time. Above our maximum STILT release height of 6 km, we used the CAM-NRT model to directly set concentrations in the profile up to a pressure height of 1 hPa. Together this generated a set of background profiles for each measurement location and time, reflecting both the effects of far-field concentrations and topographic effects on the XCH_4 measurements. We refer to these profiles as $B(z, t)$.

In addition to the CAMS-derived background described above, we also implemented a background estimation method that estimated a spatially constant background XCH_4 time series for air entering the SJV (Jones et al., 2021) and created emissions estimates using the minimum observed XCH_4 value as a constant background. These two methodologies gave similar top-down emission results as the CAMS background method and are described fully in Text S2 in Supporting Information S1.

2.5. Model XCH_4

Adding the modeled emission enhancements from STILT, $F(z, t) \times E$, and the background signals from the CAMS-NRT analysis, $B(z, t)$, gives a model estimate of the CH_4 slant mixing ratio profile at a given measurement location and time. We call this mixing ratio profile $x_{sim}(z, t)$. To create an XCH_4 model estimate, $XCH_{4,sim}$, for comparison with our measurements, we integrated $x_{sim}(z, t)$ vertically. The integration uses a vector of pressure weights, h, to capture the contribution of each profile level to $XCH_{4,sim}(t)$ as well as an averaging kernel vector, a, that accounts for the sensitivity of the XCH_4 measurement to changes from the a-priori profile, x_{ap}, used in the EM27/SUN retrieval (Wu et al., 2018). The relation between these variables is shown in Equation 1:

$$\begin{aligned} x_{sim}(z,t) &= F(z,t)\cdot(E_{dairy}+E_{non-dairy})+B(z,t) \\ XCH_{4,sim}(t) &= \sum_{level}(h\cdot a\cdot x_{sim}+(1-h\cdot a)\cdot x_{ap}) \end{aligned} \quad (1)$$

h is calculated by creating density and water profiles for our measurements using the WRF meteorological fields below 6 km and the CAMS-NRT model above 6 km. These profiles were converted to weights for the CH_4 profile using the weighting function from the GGG-2014 retrieval software (Wunch et al., 2015). The a vector is based on a look-up table from Hedelius and Wennberg (2019) and was interpolated to the solar zenith and pressure

profile used for each measurement. x_{ap} was calculated from the a-priori profile calculated by GGG-2014 for the measurements, with the profiles rescaled to match the surface pressure observed at each measurement.

2.6. Top-Down Emission Estimates

We used the hourly average XCH_4 differences (ΔXCH_4) between our instruments on each measurement day as an observational constraint to create top-down estimates of dairy and non-dairy emissions. Using a difference has advantages over XCH_4 data as measurement and modeling errors that are common to two instruments cancel out in differences and interfering effects due to emissions outside our target region and due to variations in background CH_4 concentrations should be reduced in size (Chen et al., 2016; Hedelius et al., 2018; Vogel et al., 2019; Zhao et al., 2019). Hourly averaged ΔXCH_4 observations ($\Delta XCH_{4,obs}$) were calculated from the EM27/SUN measurements with the Cantua Creek measurements used as the reference on most measurement days except on January 22nd where Terra Bella was used as the reference instrument. This was done because on this day Terra Bella showed the lowest XCH_4 values.

Plots of sample STILT trajectories on each measurement day show that on most measurement days air at each instrument enters the SJV at similar locations and times from the Pacific (see Figures S2–S7 in Supporting Information S1), suggesting that background differences between them should be small. An exception to this was on January 22nd where air from the three instruments appear to follow different paths out of the SJV which may indicate that there are larger background differences on this day. We note that these interfering effects are still modeled in our framework through the modeling of emissions throughout California and through the use and optimization of the CAMS model gradient.

These gradient observations are used in a Bayesian inversion to find multiplicative scaling factors (λ_p) on the modeled gradient signals from dairy and non-dairy emissions in the a-priori inventory and from the background ($\Delta XCH_{4,sim,d}$, $\Delta XCH_{4,sim,nd}$, and $\Delta XCH_{4,sim,b}$, respectively). Because emissions are linearly related to the ΔXCH_4 model signals, λ_p gives the optimal amount that the emissions and background gradients should be changed from the a-priori to match our observations given the uncertainties in our observations, model, and in the a-priori emissions. Under the assumption that the model gradient is linearly related to the measured gradient and that all uncertainties are normally distributed, λ_p and its error covariance matrix, S, are given by the equation from Rodgers (2000):

$$\begin{aligned} K &= [\Delta XCH_{4,sim,d}, \Delta XCH_{4,sim,nd}, \Delta XCH_{4,sim,b}] \\ \lambda_p &= \lambda_{ap} + S_{ap}K^T(K \cdot S_{ap}K^T + S_e)^{-1} \cdot (\Delta XCH_{4,obs} - K \cdot \lambda_{ap}) \\ S &= (K^T S_e^{-1} K + S_{ap}^{-1})^{-1} \end{aligned} \quad (2)$$

where λ_{ap} represents the a-priori scaling factors on the model signals, S_{ap} represents the covariance matrix of the a-priori scaling factor and S_e represents the covariance matrix of the model-measurement mismatch.

S_{ap} is taken to be a diagonal matrix, meaning we assume there is no correlation between errors in the dairy, non-dairy, and background scaling factors. The diagonal elements were calculated using a 36% standard deviation for the dairy scaling based on the uncertainty in statewide dairy emissions given in Marklein et al. (2020), a 70% standard deviation for non-dairy emissions based on estimates of CALGEM's uncertainty in the SJV by Jeong et al. (2013) and a 100% standard deviation for the background gradients, representing minimal constraints on changes to the background gradient.

S_e is also taken as a diagonal matrix with elements taken as the sum in quadrature of the model gradient uncertainty and measured gradient uncertainty. The model gradient uncertainty is dominated by transport uncertainty that can be divided into two parts: uncertainty due to horizontal transport and uncertainty due to vertical turbulence. We estimated the effect of horizontal transport uncertainty on our STILT XCH_4 enhancements by calculating the additional variance in the enhancements introduced by a stochastic wind component parameterized to model the uncertainty in our WRF wind fields in the SJV (Lin, 2005). Our full methodology is outlined in Text S1 in Supporting Information S1. The average horizontal error for the measurement days ranges from 2.5 to 3.6 ppb. We

Table 1
Meteorological Conditions Observed by ASOS Weather Stations in the SJV During the Measurement Days

Date	Temperature (°C)	Humidity (%)	Wind speed (ms^{-1})	Wind direction (°N)	Precipitation (mm)
July, 22	27 ± 6	43 ± 17	2.0 ± 0.9	307 ± 28	0
September, 12	25 ± 6	47 ± 18	2.0 ± 1.0	309 ± 93	0.03
January, 22	7 ± 4	89 ± 11	1.5 ± 0.7	91 ± 69	7.8
January, 27	10 ± 3	89 ± 10	1.8 ± 1.0	313 ± 69	0.64
January, 30	10 ± 3	89 ± 11	1.4 ± 0.6	110 ± 61	0.64
February, 3	9 ± 4	84 ± 16	5.0 ± 1.3	318 ± 12	0.47

Note. Two meters temperature and relative humidity statistics are aggregated over the 7 days prior to and on the measurement day. Accumulated rainfall is reported as a sum averaged across ASOS stations in the SJV for the 7 days prior to the measurement day. 10m wind speed and direction statistics are aggregated on each measurement day.

assessed the vertical mixing error following the methodology outlined by Wu et al. (2018). In their technique, the STILT boundary layer is uniformly rescaled by 20% during the first 24 h of the model run time and the difference in the enhancements of this perturbed model run and the unperturbed run is taken as the vertical mixing error. This error term ranges from 0.8 to 2.9 ppb over the measurement days. We note that the 20% perturbation used by this method may not be directly applicable to our SJV WRF fields. However, as XCH_4 measurements are less sensitive to boundary layer errors we did not attempt to further characterize boundary layer errors specific to our modeling setup. The measurement error is taken as the hourly standard deviation of the EM27/SUN's ΔXCH_4 measurements. The average measurement error over the measurement days ranges from 2 to 3.6 ppb. This standard deviation represents atmospheric variability in the measured XCH_4 over the hour-long averaging time. Because of the large number of measurements used to create the average, the instruments' retrieval uncertainty is relatively small. We additionally note that although we have taken S_ϵ to be diagonal, there are likely covariances in the model errors that affect the fit and neglecting these may act to make our inversion errors too conservative.

3. Results

3.1. Observed Meteorology

Meteorological conditions in the SJV were recorded on all our measurement days by 15 surface weather stations in the ASOS network (retrieved from https://mesonet.agron.iastate.edu/request/download.phtml). A map of these stations is shown in Figure S8 in Supporting Information S1. We aggregated data from these stations to estimate average meteorological conditions and their variability over the SJV during the time periods on and preceding our measurement days. These variables are shown in Table 1 and are used to help interpret the EM27/SUN measurements. Wind direction and speed at 10 m are reported as an SJV wide average over the night before the measurement day, defined as beginning at 20:00 local time, and the end of the measurement day at 17:00 local time. This period was based on Figure 7 which shows that most of the XCH_4 enhancements measured by the instruments are released over this period. Temperature, humidity and rainfall statistics are reported as SJV wide averages over the 7 days prior to and including the measurement days. This was based on the assumption that changes to dairy emissions due to these variables should occur on the order of days as they should affect conditions within the liquid manure systems.

As expected, temperature in the SJV is highest during the summer (July and September measurement days) and declines on the winter measurement days. Humidity and rainfall, in contrast, are highest on the winter measurement days and. Wind speed is low on all measurement days except on February 3rd when average wind speeds are 5 m/s. The average wind direction is from the northwest on all days except on January 22nd and 30th when it is on average from the east. All the meteorological variables fall within 1σ of the 30 day SJV-wide average centered around each measurement day except for the wind speed in February which is 2.8σ higher than the average winds.

Because the accuracy of the model wind fields is important for determining the accuracy of a transport simulation, we also compared our WRF fields to the 10m wind measurements from the ASOS network in the SJV. This allows us to assess the quality of the STILT model on each measurement day. The comparison is shown in Figure 3. On most of the measurement days, there is a good correlation between the WRF and ASOS winds and

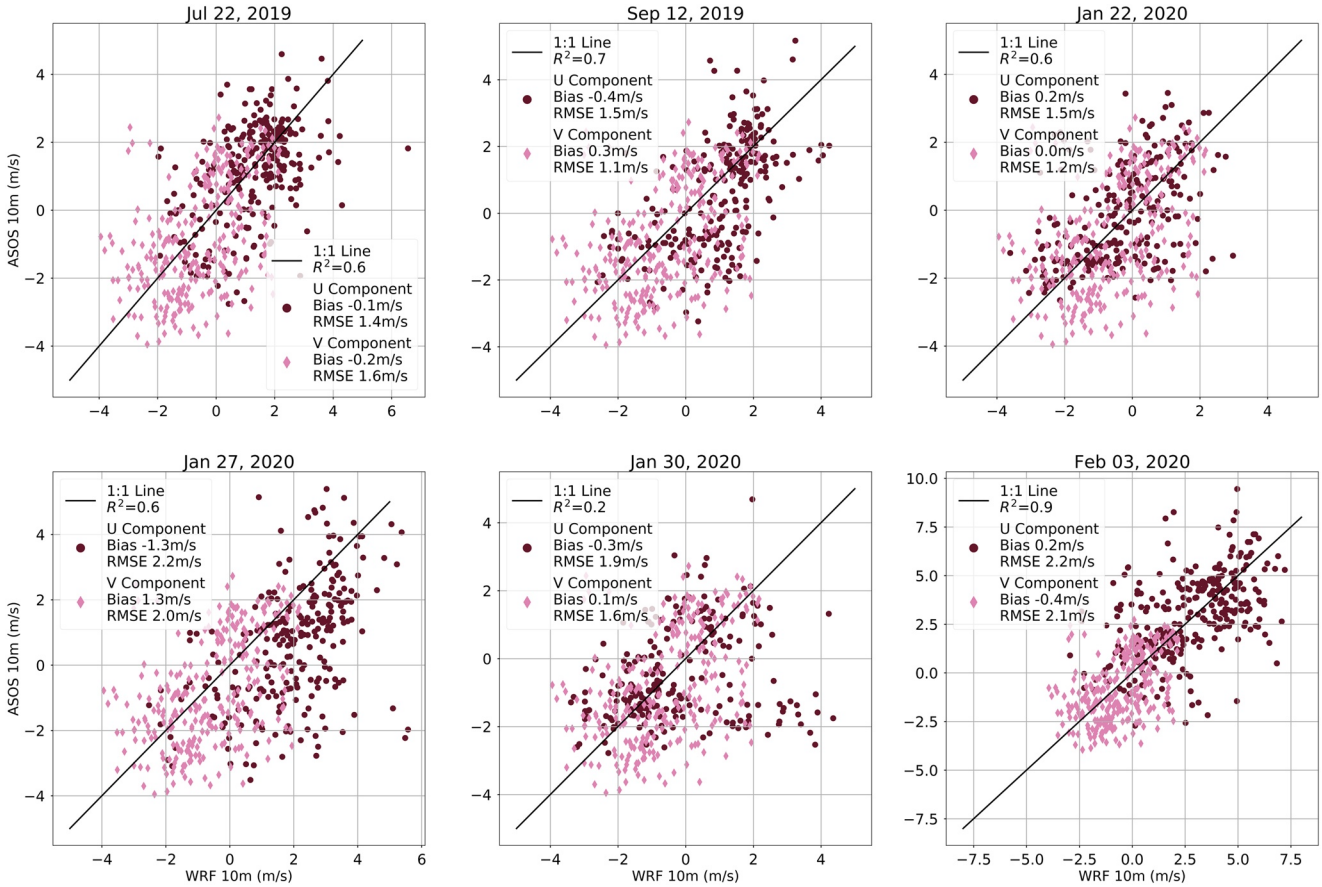

Figure 3. Comparison of 10m wind from our WRF meteorological fields with the ASOS network in the SJV. The comparison is done using data from 21:00 local time on the night before the measurements to 18:00 local on the day of the measurements. The north-south (v) and east-west (u) wind components are shown in different colors on the plot.

biases are typically small. The exceptions to this are the high bias in both wind components observed on January 27th and the low correlation with the ASOS network on January 30th. The deficiency in the wind fields may indicate problems in the model signals on these days but our meterological uncertainty analysis should model the effect of the higher random error on January 30th.

3.2. STILT Model Results

Comparisons between the optimized model ΔXCH_4 signals and the measured EM27/SUN signals are shown in Figure 4 for each of the 6 sampling days. We find that on all measurement days except January 30th, there is a good fit between our model results and the measurements as measured by the reduction in uncertainty in the a-posteriori dairy emission scaling factors. Notably, our top-down inversion reduces the uncertainty on the emissions by a factor of 2 or more compared to the a-priori uncertainty (0.36) on most days, showing that the observations can constrain the emissions. The RMSE between the optimized model and the measurements varies over the measurement days and is smallest on the July, September, and February days. This indicates a better model fit and stronger constraints on emissions on these days. On January 30th, the fit was much worse by both metrics, with the model failing to capture the enhancements observed at the Helm's Corner site in the morning. We attribute this to errors in the WRF model, evidenced by the poor correlation between the WRF 10 m winds and weather station observations in the SJV on this day (see Figure 3).

On the 2 summer measurement days, July 22nd and September 12th, we found top-down scaling factors on the a-priori dairy emissions of 84 ± 13% (95% confidence interval [CI] = 58%–110%) and 84 ± 11% (95% CI = 62%–105%) respectively. On the winter measurement days, January 22, January 27, January 30, and February 3,

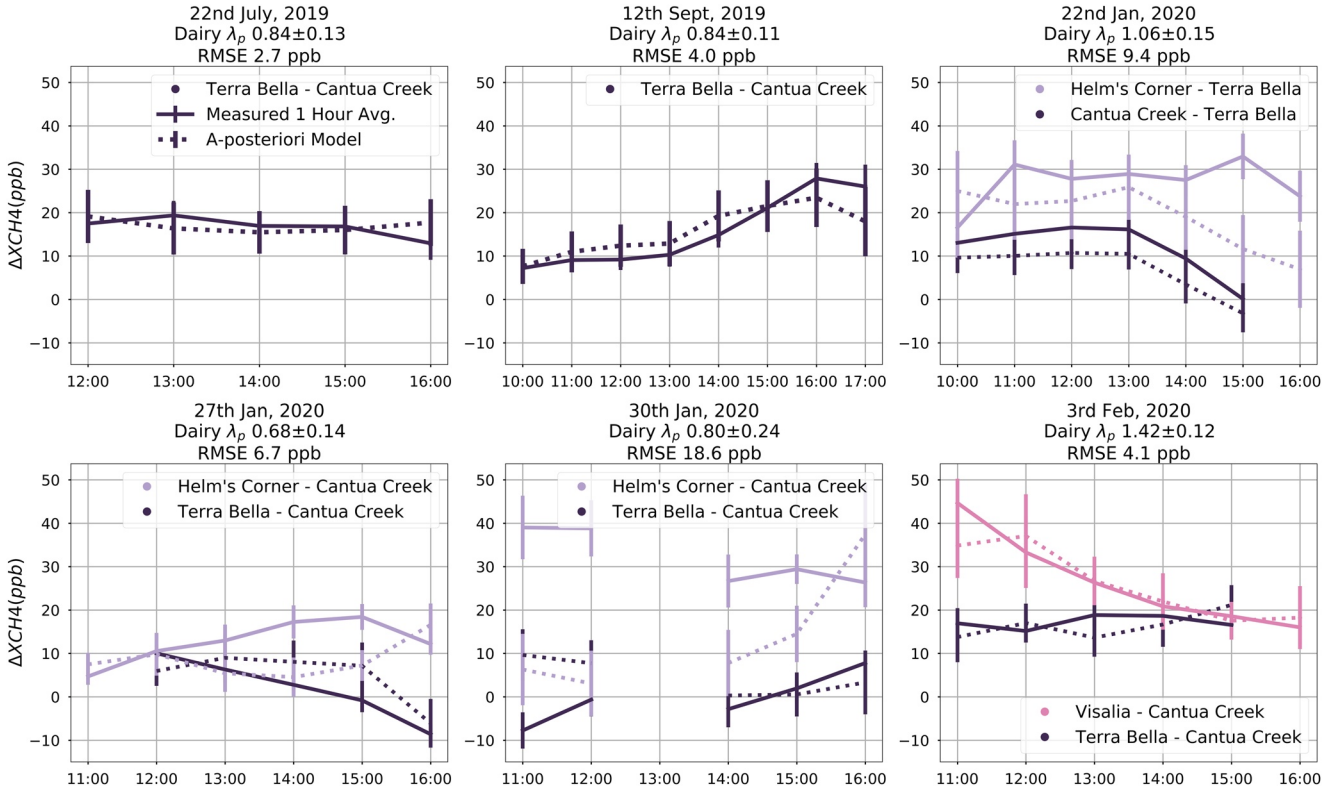

Figure 4. Comparison of measured ΔXCH_4 signal to our a-posteriori model signal after a Bayesian inversion. Error bars on the measured signal are the 1 hr standard deviation of our measured gradients. The error on the optimized model signal represents a bootstrap standard deviation of the a-posteriori model prediction distribution. Lines in the plots are colored by measurement locations. Solid lines represent measured $\Delta XCH_{4,obs}$ and dotted lines represent the a-posteriori modeled $\Delta XCH_{4,sim}$. Times are in the local timezone (US/Pacific). The root mean square error between the optimized model and measurements as well as the a-posteriori dairy emissions scaling factor are also shown.

the top-down scaling factors on dairy emissions were 106 ± 15% (95% CI = 76%–136%), 68 ± 15% (95% CI = 39%–97%), 80 ± 23% (95% CI = 36%–125%) and 141 ± 12% (95% CI = 117%–165%), respectively.

The a-priori non-dairy emissions were not significantly changed on any of the measurement days and there is minimal reduction in these emissions' uncertainty compared to the a-priori. This indicates that non-dairy emissions are not constrained by our measurements and this is expected given the small amount of non-dairy emissions in the study area. Finally, the a-priori background gradient is not significantly changed on the July 22, September 12 (summer), and February 3 (winter) measurement days indicating that the background gradient does not have a strong effect on the inversion on these days. In contrast, on January 22, 27, and 30, the inversion significantly changes the background gradient between the instruments indicating that the CAMS model background gradient needs to be altered to match the measurements on these days. The adjustment to the model background gradient is especially large on January 22 for the Cantua Creek and Terra Bella gradient and is on the order of 500%. This may reflect a difficulty in CAMS-NRT modeling the differences in background XCH_4 caused by the more distinct paths air arriving at each instrument takes entering the SJV on this day (Figure S4 in Supporting Information S1).

3.3. Emission Sensitivity Area

Our top-down analysis gives single top-down scaling factors for dairy and non-dairy emissions but does not give information on the spatial region they apply to. Because of this, it is necessary to determine which locations in the a-priori inventory contribute to the ΔXCH_4 signals before inter-comparing our results or comparing it to other emission estimates. We did this by creating contribution maps showing how much ΔXCH_4 each grid cell in the a-priori emissions contributed to the STILT model signals as shown in Figure 5. They show that on all the measurement days a large proportion of the modeled ΔXCH_4 comes from emissions from dairy farms in Tulare and Kings counties. This was the area that we targeted with our measurement network and the maps suggest that

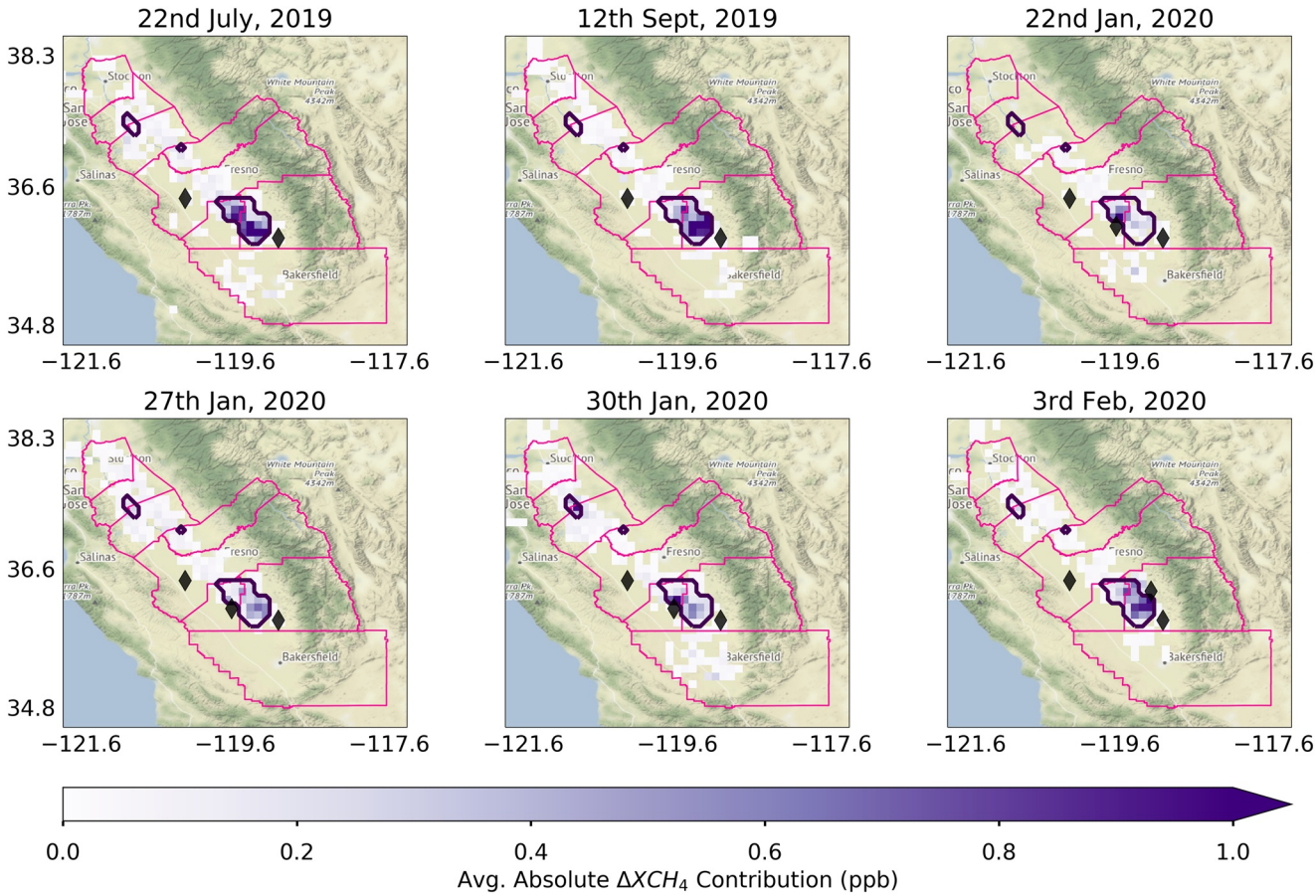

Figure 5. ΔXCH_4 contribution of different grid cells in the a-priori inventory to average STILT model signals on each measurement day. Black diamonds show the EM27/SUN measurement locations. The dashed black outline shows our emission sensitivity area defined as the region that on average contributes ≥0.1 ppb to the model signal on measurement days. The pink outline shows the San Joaquin Valley's county boundaries. The Stamen Terrain base map is used.

the scaling factors on these days apply to roughly the same area. We explicitly define this area by selecting grid cells in the a-priori inventory that on average contribute at least 0.1 ppb to the modeled ΔXCH_4 signal over the measurement days.

This sensitivity area is outlined in Figure 5. It contains 585 dairy farms out of 1,317 in the SJV and covers approximately 3×10^3 km^2. Liquid manure management in waste ponds is the predominant manure management method among these dairy farms and they contain a mix of freestall and dry lot animal housing (Marklein et al., 2020; Meyer et al., 2011). At least 60% of the modeled signal on each of these days comes from this area and at least 90% of its total emissions are from the dairy sector. The a-posteriori scaling factors derived from the inversion are applied only to a-priori emissions in this area giving top-down emission estimates for each day. These are shown in Figure 6. This restriction ensures that the scaling factors are applied only to areas that our measurements are sensitive to.

3.4. Temporal Sensitivity to Emissions

Similar to the above spatial analysis, we can use our STILT footprints to estimate the time period when the CH_4 emissions we measure were released. Determining the sensitivity time of our top-down emissions is useful as work by Wood et al. (2013) on dairy manure emissions and Vaughn et al. (2018) on fossil fuel emissions suggest that differences in the time period different methods estimate emissions for can create discrepancies between them.

Figure 7 shows the contribution of emissions released at different times to the modeled absolute ΔXCH_4 averaged over each measurement day. This plot suggests that our XCH_4 measurements have a broad temporal sensitivity

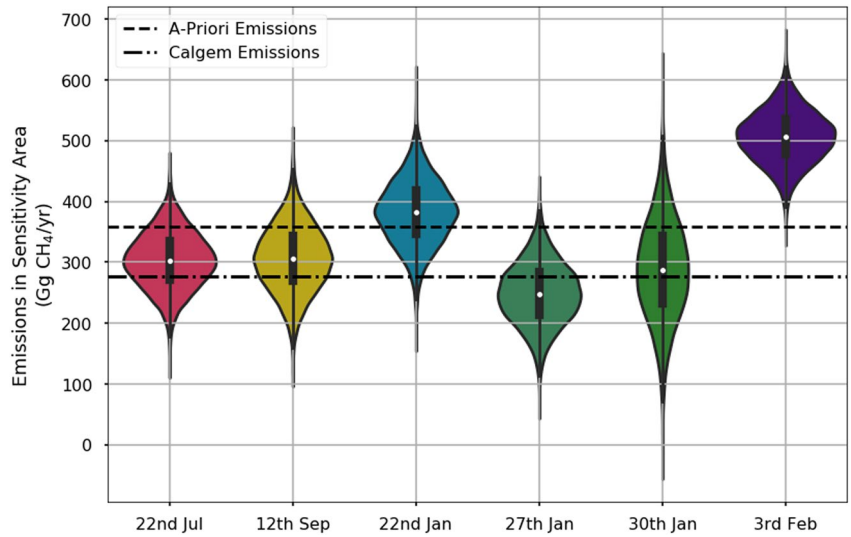

Figure 6. A-posteriori distribution of total CH_4 emission in the sensitivity area for different measurement days using our top-down inversions. The box plot in the center of the distributions shows the 25th and 75th percentiles and outlier points in black. The median is shown in white. A-priori emissions based on CALGEM and Marklein et al. (2020) are shown as a dashed line.

spanning several hours and that their peak sensitivity ranges from 02:00 on the night before the measurement day to 07:00 on the morning of the measurement day. Although our measurements were mostly taken in the afternoon, this result is not unexpected. Because of the large size of our sensitivity area (10s of km) and the low wind speeds and ventilation rates present in the SJV, it takes several hours from entering the SJV for air to flow to the downwind sites. This allows the instruments to measure emissions released overnight and in the morning. Interestingly, Wood et al. (2013) found that the lowest deviation from diurnally averaged emission rates in dairy manure lagoons is realized when the top-down emissions are sensitive to emissions released between 18:00 and 08:00. This suggests that our measurements may have minimal bias due to diurnal variations in the dairy farms'

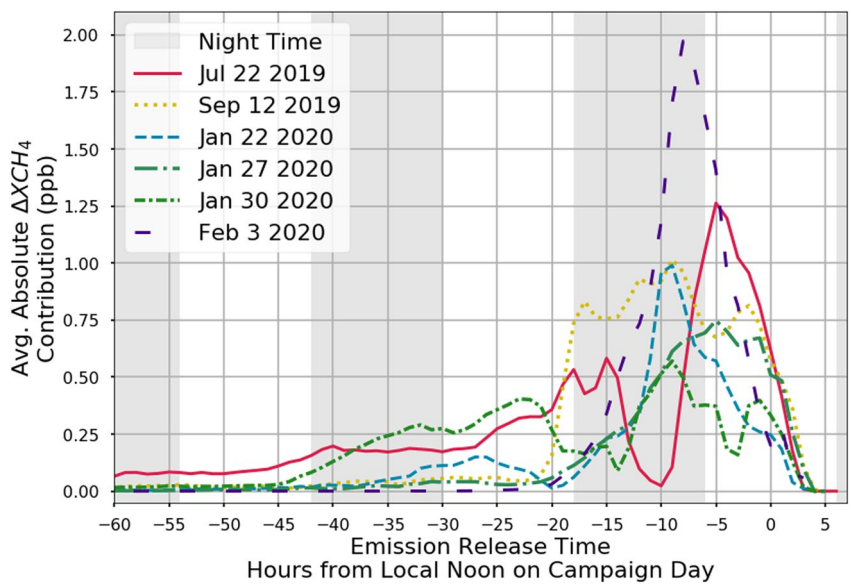

Figure 7. Modeled contribution of emissions released at different times to absolute ΔXCH_4 signals averaged over each measurement day. On days with three instruments, the emission contribution time series of the two gradients are averaged together. Each measurement days' contribution curve is shown in a different color.

emissions. However, the broad temporal sensitivity also means that it is difficult to assess if there is coherent diurnal variability in the SJV's emissions from our measurements.

4. Discussion

Our analysis finds that the dairy emissions on the winter measurement days (January 22nd 371 ± 54 Gg/yr, January 27th 237 ± 52 Gg/yr, January 30th 281 ± 81 Gg/yr, and February 3rd 491 ± 43 Gg/yr) are comparable to or higher than dairy emissions on the 2 summer measurement days (July 22nd 291 ± 47 Gg/yr and September 12th 292 ± 38 Gg/yr). Although temperature is an important driver of dairy CH_4 emissions and would be expected to reduce dairies' manure emissions in the winter, this finding suggests that other factors act to increase dairy emissions in our study area over the winter measurement days.

We can estimate the expected effect of temperature on manure dairy emissions over the measurement days using an Arrhenius temperature relationship (Safley & Westerman, 1988) driven by 7 day averaged SJV surface temperatures from the ASOS stations. The change in manure emissions can then be converted to the relative change in total dairy emissions using the ratio of manure emissions to total dairy emissions in the a-priori inventory (47%). This analysis predicts that temperature changes should cause emissions on the winter days to be approximately 60% of emissions on July 22nd or 174 Gg/yr. None of our top-down emission estimates on the winter measurements days overlap with this value within the 1σ uncertainty and the emissions on January 22nd, February 3rd are higher than this value within their 2σ uncertainty. This difference from the decline in emissions predicted from temperature changes suggests that other factors act to control seasonality in the SJV's dairy CH_4 emissions. Additionally, dairy emissions on the second summer day (September 12) should be 89% of emissions on the first summer day due to the temperature effects and this overlaps within the 1σ error with the ratio of top-down emission we measured (100 ± 20%).

This result in the central SJV on our measurement days is in accord with other studies which showed no significant seasonality in California's statewide dairy emissions (Jeong et al., 2016) and which showed increases in winter emissions in the northern SJV relative to other seasons (Johnson et al., 2016). Additionally, a study by Leytem et al. (2017) at a group of US dairy farms found that non-temperature factors could act to mask seasonal temperature effects on emissions. We note that aside from temperature changes, there are dramatic changes in precipitation patterns in the SJV between the summer and winter (see Table 1). Rainfall could act to increase the SJV's dairy emissions by altering the input of manure to anaerobic liquid waste storage systems through management decisions (Meyer et al., 2019). Also, rainfall has been shown to increase individual dairy farms' CH_4 emissions by enhancing the agitation of liquid manure ponds (Leytem et al., 2017) and could also increase emissions by expanding the emitting area of the manure ponds (Petersen, 2018). With our time-limited campaign data set, we can not directly attribute the higher than expected winter emissions to any one factor. However, the result suggests a need for measurements at regional scales like ours as well as on individual dairy facilities to constrain the seasonally varying effects of temperature, moisture, and dairy management on the SJV's dairy emissions.

During the winter, the SJV's natural gas consumption is about 3.5 times higher than in the summer (Pacific Gas & Electric, 2019). Higher winter natural gas emissions could contribute to total emissions in the SJV being higher than expected rather than dairy emissions. To assess this explanation, we ran a sensitivity test by artificially increasing the size of natural gas emissions in the a-priori inventory by a factor of 5. The scaling factors recovered for this perturbed a-priori overlap within 1σ error with the scaling factors calculated with our unperturbed a-priori emissions and do not show a decline in dairy emissions in the winter. This suggests that natural gas emissions do not contribute to our observation of relatively high winter emissions.

Interestingly, our measurements also show evidence of interday variability in emissions. Top-down emissions on February 3rd are higher than emissions on all the other measurement days at the 2σ uncertainty level except on January 22nd where it is higher at the 1σ uncertainty level. This may be related to the anomalously high wind speed measured across the SJV on the night before and during February 3rd (see Table 1). Leytem et al. (2017) and Grant et al. (2015) both reported strong correlations between manure methane emissions and wind speed at individual facilities that they attributed to enhanced agitation and release of CH_4 from the liquid manure ponds. This effect could be driving a coherent increase in emissions over all the dairy farms in our sensitivity area causing the higher top-down emissions. Given that we are restricted to 6 measurement days, it is difficult to fully assess the importance of intermittent emission events on longer term emissions or to unambiguously attribute the

higher emissions to wind speed. Work by Duren et al. (2019) in the SJV also found that emissions at individual dairies in the region were intermittent in time. This along with our regional finding suggests a need for reanalysis of existing long term data sets, such as the GOSAT and TROPOMI satellite XCH_4 record and the CARB in-situ tower record as well as new long term sampling in the SJV to further investigate the drivers of interday variability and to determine its importance to emissions in the region.

Our top-down emissions in the sensitivity area all overlap with the bottom-up emissions in the a-priori inventory within their respective 1σ uncertainties. Since the a-priori was constructed with annual bottom-up emissions this means that both the variability in our days' top-down estimates and their difference from the a-priori fall within the overall uncertainty of the annual bottom-up emissions. Our top-down emissions also overlap with the emissions from the CALGEM inventory within an assumed 70% 1σ error on CALGEM's total emissions. Other bottom-up inventories in the region such as the EPA inventory (Maasakkers et al., 2016) have known issues in localizing emissions in the SJV (Marklein et al., 2020) that preclude them from comparison to emission in our sensitivity area.

We also compared our EM27/SUN XCH_4 based emissions to three other studies that estimated top-down emissions in the SJV using different measurement techniques: an aircraft-based estimate by Cui et al. (2017), an in-situ tower-based estimate by Jeong et al. (2016), and a satellite XCH_4-based estimate by Turner et al. (2015). Cui et al. (2017) created emission estimates in the southern SJV (encompassing our sensitivity area) based on boundary layer CH_4 mixing ratio data collected on four aircraft flights during the spring and early summer of 2010. Jeong et al. (2016) used near-surface mixing ratio measurements from CARB's regional tower network from June 2013 to May 2014 to make an estimate of the entire SJV's annual emissions. For these studies, we applied the average ratio between their top-down emissions and CALGEM to CALGEM's emissions in our sensitivity area. We also assumed that the uncertainty they reported for these larger regions applied to the downscaled emissions. Turner et al. (2015) reported annual emissions across North America at a $0.5° \times 0.667°$ resolution using XCH_4 soundings from the GOSAT satellite from 2009 to 2011. We summed emissions in grid cells in their top-down emission map that overlapped with our sensitivity area for comparison with our emissions and assumed that the uncertainty they reported for California-wide emissions applied to this area.

We note that there are difficulties inherent in these comparisons, particularly in downscaling emissions, in the multi-year difference in when these measurements were collected, and in the differences in the timescales and time periods the top-down estimates apply to. Despite this, an error-weighted average of emissions across our measurement days overlaps within 1σ error with the other top-down estimates as shown in Figure 8. On individual

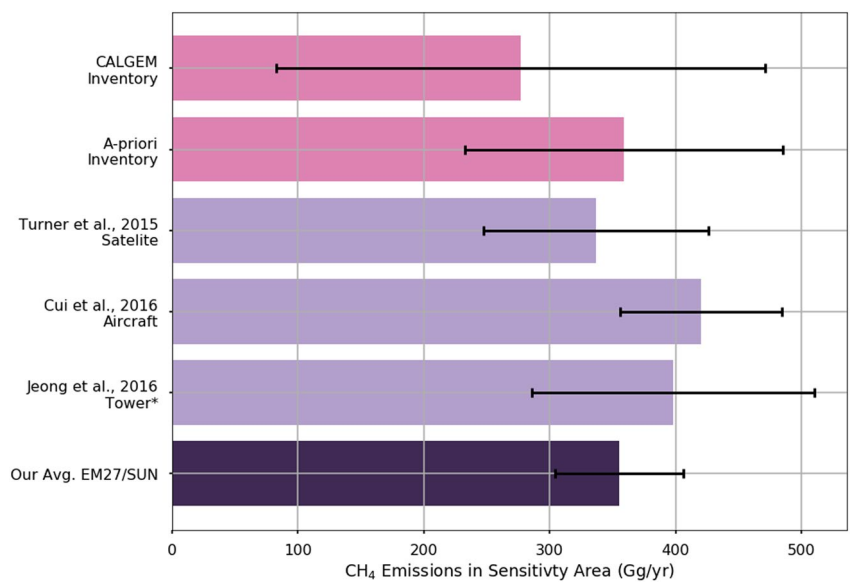

Figure 8. Comparison of emissions in our sensitivity area from different studies. An error weighted average of our EM27/SUN emissions is shown in dark purple. Emissions from other top-down studies are shown in light purple and emissions from bottom-up inventories are shown in pink. Error bars on the plot represent 1σ uncertainty except for Jeong et al. (2016)* where the error represents a 95% CI.

days, emissions all overlap within their respective 95% CIs with the other estimates. However, emissions on the summer days and January 27th fall below the 1σ uncertainty band of Cui et al. (2017) results and emissions on February 3rd fall above the 1σ uncertainty band of Turner et al. (2015) results. Despite this, the overall consistency of our results suggests that our EM27/SUN methodology is able to retrieve emissions correctly and suggests that emissions in the central SJV region we were sensitive to are similar to emissions in the wider SJV.

5. Conclusions

We reported EM27/SUN ΔXCH_4 across the SJV during the summer and winter and used them to constrain dairy CH_4 emissions using WRF–STILT inversions. We find that our measurements capture the influence of CH_4 emissions from a large grouping of dairies in the central SJV, a region with low constraints on emissions, on all of our measurement days and are sensitive to relatively similar times of day. Our measurements also span the summer and winter and we find that CH_4 emissions in the SJV are much higher during the winter measurement days than would be expected from the temperature effects used in the current national scale CH_4 inventories of dairy emissions. We also observe significant interday variability in our measurements. These results suggest that seasonal management changes in the dairies, wind agitation of manure ponds, and other biogeochemical responses in the region could be important factors controlling emissions. They also demonstrate a need for more long-term measurements to constrain the size and causes of variability in the SJV and to determine its importance on long-term emissions. On average we find top-down emissions of 347 $\pm$ 46 Gg/yr in our sensitivity area in the central SJV, representing a scaling factor of 125 $\pm$ 17% on CALGEM's emissions in the area. These average emissions were also found to fall within the uncertainty ranges of previous top-down and bottom-up inferences.

Given the importance of the SJV region for statewide CH_4 emissions, our study underscores the need for longer term and more varied measurements of CH_4 emissions in the SJV to fully characterize the factors controlling its emissions. In particular, reanalysis of existing long-term measurements such as the decade long XCH_4 record from the GOSAT satellite and the CARB in-situ tower network could provide further insight into controls on emissions in the SJV. Further analysis at the individual dairy facility scale would also be useful for resolving questions about controls on emissions. Our analysis also demonstrates that the EM27/SUN instruments can constrain regional emissions to a relatively good accuracy compared to other techniques and suggest that they can play a role in further studies of CH_4 emissions in the SJV.

Acknowledgments
This study was funded by the University of California Office of the President's Grant LFR-18-548581. Work at Lawrence Berkeley National Laboratory was partially supported by Contractor Supporting Research (CSR) funding from Berkeley Lab, provided by the Director, Office of Science, under Contract No. DE-AC02-05CH11231 with the U.S. Department of Energy. The authors also thank M. Rodriguez, Z. Zhu, D. Meyer, A. Velasco, I. Vicencio and D. Frausto-Vicencio for their help with facilitating and performing the field measurements; J. Podolske for help with conducting the Armstrong TCCON measurements; Taylor Jones for sharing his code to generate a STILT receptor list for the EM27/SUN; Jacob Hedelius, Nicole Jacobs, Nasrin Pak, Debra Wunch for guidance on using the EM27/SUN's and their retrievals; Alex Turner for providing the emission map from Turner et al. (2015); I. Lino for constructing cooling enclosures for the EM27/SUN's and M. Rodriguez, K. Heerah and V. Carranza for proofreading the draft. The authors thank LBNL's Cluster Computing Program and William Porter for the assistance running the WRF-STILT models on the LBNL-Lawrencium and UCR-Aldo clusters respectively.

Data Availability Statement

The EM27/SUN retrievals used in this study and the STILT footprints are available at https://osf.io/gnfb4/.

References

Arndt, C., Leytem, A., Hristov, A., Zavala-Araiza, D., Cativiela, J., Conley, S., et al. (2018). Short-term methane emissions from 2 dairy farms in California estimated by different measurement techniques and US Environmental Protection Agency inventory methodology: A case study. *Journal of Dairy Science*, *101*(12), 11461–11479. https://doi.org/10.3168/jds.2017-13881

Bagley, J. E., Jeong, S., Cui, X., Newman, S., Zhang, J., Priest, C., et al. (2017). Assessment of an atmospheric transport model for annual inverse estimates of California greenhouse gas emissions. *Journal of Geophysical Research: Atmospheres*, *122*(3), 1901–1918. https://doi.org/10.1002/2016jd025361

CARB. (2017). *California's 2017 climate change scoping plan*. California Air Resources Board. Retrieved from https://ww3.arb.ca.gov/cc/scopingplan/scoping_plan_2017.pdf

CARB. (2019). *GHG current California emission inventory data*. California Air Resources Board. Retrieved from https://ww2.arb.ca.gov/ghg-inventory-data

CDFA. (2020). *California agriculture statistics review 2018–2019*. California Department of Agriculture. Retrieved from https://www.cdfa.ca.gov/statistics/PDFs/2018-2019AgReportnass.pdf

Chen, J., Viatte, C., Hedelius, J. K., Jones, T., Franklin, J. E., Parker, H., et al. (2016). Differential column measurements using compact solar-tracking spectrometers. *Atmospheric Chemistry and Physics*, *16*(13), 8479–8498. https://doi.org/10.5194/acp-16-8479-2016

Cui, Y. Y., Brioude, J., Angevine, W. M., Peischl, J., McKeen, S. A., Kim, S.-W., et al. (2017). Top-down estimate of methane emissions in California using a mesoscale inverse modeling technique: The San Joaquin Valley. *Journal of Geophysical Research: Atmospheres*, *122*(6), 3686–3699. https://doi.org/10.1002/2016jd026398

Cui, Y. Y., Vijayan, A., Falk, M., Hsu, Y.-K., Yin, D., Chen, X. M., et al. (2019). A multiplatform inversion estimation of statewide and regional methane emissions in California during 2014–2016. *Environmental Science & Technology*, *53*(16), 9636–9645. https://doi.org/10.1021/acs.est.9b01769

Dlugokencky, E. J., Nisbet, E. G., Fisher, R., & Lowry, D. (2011). Global atmospheric methane: Budget, changes and dangers. *Philosophical Transactions of the Royal Society A: Mathematical, Physical & Engineering Sciences*, *369*(1943), 2058–2072. https://doi.org/10.1098/rsta.2010.0341

Duren, R. M., Thorpe, A. K., Foster, K. T., Rafiq, T., Hopkins, F. M., Yadav, V., et al. (2019). California's methane super-emitters. *Nature*, *575*(7781), 180–184. https://doi.org/10.1038/s41586-019-1720-3

Etminan, M., Myhre, G., Highwood, E. J., & Shine, K. P. (2016). Radiative forcing of carbon dioxide, methane, and nitrous oxide: A significant revision of the methane radiative forcing. *Geophysical Research Letters*, *43*(24), 12614–12623. https://doi.org/10.1002/2016gl071930

Fasoli, B., Lin, J. C., Bowling, D. R., Mitchell, L., & Mendoza, D. (2018). Simulating atmospheric tracer concentrations for spatially distributed receptors: Updates to the Stochastic Time-Inverted Lagrangian Transport model's R interface (STILT-R version 2). *Geoscientific Model Development*, *11*(7), 2813–2824. https://doi.org/10.5194/gmd-11-2813-2018

Fiore, A. M., West, J. J., Horowitz, L. W., Naik, V., & Schwarzkopf, M. D. (2008). Characterizing the tropospheric ozone response to methane emission controls and the benefits to climate and air quality. *Journal of Geophysical Research*, *113*(D8). https://doi.org/10.1029/2007jd009162

Fischer, M. L. (2017). *CALGEM prior emissions model*. Lawrence Berkley National Laboratory. Retrieved from http://calgem.lbl.gov/inventory_estimates.html

Gisi, M., Hase, F., Dohe, S., Blumenstock, T., Simon, A., & Keens, A. (2012). XCO2 measurements with a tabletop FTS using solar absorption spectroscopy. *Atmospheric Measurement Techniques*, *5*(11), 2969–2980. https://doi.org/10.5194/amt-5-2969-2012

Grant, R. H., Boehm, M. T., & Bogan, B. W. (2015). Methane and carbon dioxide emissions from manure storage facilities at two free-stall dairies. *Agricultural and Forest Meteorology*, *213*, 102–113. https://doi.org/10.1016/j.agrformet.2015.06.008

Hase, F., Frey, M., Blumenstock, T., Groß, J., Kiel, M., Kohlhepp, R., et al. (2015). Application of portable FTIR spectrometers for detecting greenhouse gas emissions of the major city Berlin. *Atmospheric Measurement Techniques*, *8*(7), 3059–3068. https://doi.org/10.5194/amt-8-3059-2015

Hedelius, J. K., Feng, S., Roehl, C. M., Wunch, D., Hillyard, P. W., Podolske, J. R., et al. (2017). Emissions and topographic effects on column CO2 (XCO2) variations, with a focus on the Southern California megacity. *Journal of Geophysical Research: Atmospheres*, *122*(13), 7200–7215. https://doi.org/10.1002/2017jd026455

Hedelius, J. K., Liu, J., Oda, T., Maksyutov, S., Roehl, C. M., Iraci, L. T., et al. (2018). Southern California megacity CO2, CH4, and CO flux estimates using ground- and space-based remote sensing and a Lagrangian model. *Atmospheric Chemistry and Physics*, *18*(22), 16271–16291. https://doi.org/10.5194/acp-18-16271-2018

Hedelius, J. K., Viatte, C., Wunch, D., Roehl, C. M., Toon, G. C., Chen, J., et al. (2016). Assessment of errors and biases in retrievals of XCO2, XCH4, XCO, and XN2O from a 0.5 cm–1 resolution solar-viewing spectrometer. *Atmospheric Measurement Techniques*, *9*(8), 3527–3546. https://doi.org/10.5194/amt-9-3527-2016

Hedelius, J. K., & Wennberg, P. O. (2019). *Em27/SUN GGG interferogram processing suite*. Califronia Insitute of Technology. Retrieved from https://data.caltech.edu/records/306

Husted, S. (1994). Seasonal variation in methane emission from stored slurry and solid manures. *Journal of Environmental Quality*, *23*(3), 585–592. https://doi.org/10.2134/jeq1994.00472425002300030026x

Inness, A., Ades, M., Agustí-Panareda, A., Barré, J., Benedictow, A., Blechschmidt, A.-M., et al. (2019). The CAMS reanalysis of atmospheric composition. *Atmospheric Chemistry and Physics*, *19*(6), 3515–3556. https://doi.org/10.5194/acp-19-3515-2019

Jeong, S., Hsu, Y.-K., Andrews, A. E., Bianco, L., Vaca, P., Wilczak, J. M., & Fischer, M. L. (2013). A multitower measurement network estimate of California's methane emissions. *Journal of Geophysical Research: Atmospheres*, *118*(19), 11339–11351. https://doi.org/10.1002/jgrd.50854

Jeong, S., Newman, S., Zhang, J., Andrews, A. E., Bianco, L., Bagley, J., et al. (2016). Estimating methane emissions in California's urban and rural regions using multitower observations. *Journal of Geophysical Research: Atmospheres*, *121*(21), 13031–13049. https://doi.org/10.1002/2016jd025404

Johnson, M. S., Xi, X., Jeong, S., Yates, E. L., Iraci, L. T., Tanaka, T., et al. (2016). Investigating seasonal methane emissions in Northern California using airborne measurements and inverse modeling. *Journal of Geophysical Research: Atmospheres*, *121*(22), 13753–13813. https://doi.org/10.1002/2016jd025157

Jones, T. S., Franklin, J. E., Chen, J., Dietrich, F., Hajny, K. D., Paetzold, J. C., et al. (2021). Assessing urban methane emissions using column observing portable FTIR spectrometers and a novel Bayesian inversion framework. *Atmospheric Chemistry and Physics Discussions*, *21*(17), 13131–13147. https://doi.org/10.5194/acp-2020-1262

Keppel-Aleks, G., Wennberg, P. O., & Schneider, T. (2011). Sources of variations in total column carbon dioxide. *Atmospheric Chemistry and Physics*, *11*(8), 3581–3593. https://doi.org/10.5194/acp-11-3581-2011

Kille, N., Chiu, R., Frey, M., Hase, F., Sha, M. K., Blumenstock, T., et al. (2019). Separation of methane emissions from agricultural and natural gas sources in the Colorado Front Range. *Geophysical Research Letters*, *46*(7), 3990–3998. https://doi.org/10.1029/2019gl082132

Kort, E. A., Frankenberg, C., Costigan, K. R., Lindenmaier, R., Dubey, M. K., & Wunch, D. (2014). Four corners: The largest US methane anomaly viewed from space. *Geophysical Research Letters*, *41*(19), 6898–6903. https://doi.org/10.1002/2014gl061503

Lauvaux, T., & Davis, K. J. (2014). Planetary boundary layer errors in mesoscale inversions of column-integrated CO_2 measurements. *Journal of Geophysical Research: Atmospheres*, *119*(2), 490–508. https://doi.org/10.1002/2013jd020175

Leytem, A., Bjorneberg, D., Koehn, A., Moraes, L., Kebreab, E., & Dungan, R. (2017). Methane emissions from dairy lagoons in the western United States. *Journal of Dairy Science*, *100*(8), 6785–6803. https://doi.org/10.3168/jds.2017-12777

Lin, J. C. (2003). A near-field tool for simulating the upstream influence of atmospheric observations: The stochastic time-inverted Lagrangian transport (stilt) model. *Journal of Geophysical Research*, *108*(D16), ACH 2-1–ACH 2-17. https://doi.org/10.1029/2002jd003161

Lin, J. C. (2005). Accounting for the effect of transport errors on tracer inversions. *Geophysical Research Letters*, *32*(1). https://doi.org/10.1029/2004gl021127

Luther, A., Kleinschek, R., Scheidweiler, L., Defratyka, S., Stanisavljevic, M., Forstmaier, A., et al. (2019). Quantifying CH_4 emissions from hard coal mines using mobile sun-viewing Fourier transform spectrometry. *Atmospheric Measurement Techniques*, *12*(10), 5217–5230. https://doi.org/10.5194/amt-12-5217-2019

Maasakkers, J. D., Jacob, D. J., Sulprizio, M. P., Turner, A. J., Weitz, M., Wirth, T., et al. (2016). Gridded national inventory of U.S. methane emissions. *Environmental Science & Technology*, *50*(23), 13123–13133. https://doi.org/10.1021/acs.est.6b02878

Makarova, M. V., Alberti, C., Ionov, D. V., Hase, F., Foka, S. C., Blumenstock, T., et al. (2021). Emission monitoring mobile experiment (EMME): An overview and first results of the St. Petersburg Megacity Campaign 2019. *Atmospheric Measurement Techniques*, *14*(2), 1047–1073. https://doi.org/10.5194/amt-14-1047-2021

Marklein, A. R., Meyer, D., Fischer, M. L., Jeong, S., Rafiq, T., Carr, M., & Hopkins, F. M. (2020). Facility scale inventory of dairy methane emissions in California: Implications for mitigation. *Earth System Science Data*, *13*(3), 1151–1166. https://doi.org/10.5194/essd-2020-133

McKain, K., Wofsy, S. C., Nehrkorn, T., Eluszkiewicz, J., Ehleringer, J. R., & Stephens, B. B. (2012). Assessment of ground-based atmospheric observations for verification of greenhouse gas emissions from an urban region. *Proceedings of the National Academy of Sciences of the United States of America*, *109*(22), 8423–8428. https://doi.org/10.1073/pnas.1116645109

Meyer, D., Heguy, J., Karle, B., & Robinson, P. (2019). *Characterize physical and chemical properties of manure in California dairy systems to improve greenhouse gas emission estimates*. California Air Resources Board. Retrieved from https://ww2.arb.ca.gov/sites/default/files/classic//research/apr/past/16rd002.pdf

Meyer, D., Price, P., Rossow, H., del Rio, N. S., Karle, B., Robinson, P., et al. (2011). Survey of dairy housing and manure management practices in California. *Journal of Dairy Science*, *94*(9), 4744–4750. https://doi.org/10.3168/jds.2010-3761

Miller, S. M., Wofsy, S. C., Michalak, A. M., Kort, E. A., Andrews, A. E., Biraud, S. C., et al. (2013). Anthropogenic emissions of methane in the United States. *Proceedings of the National Academy of Sciences of the United States of America*, *110*(50), 20018–20022. https://doi.org/10.1073/pnas.1314392110

Myhre, G., Shindell, D., Bréon, F.-M., Collins, W., Fuglestvedt, J., Huang, J., & Zhang, H. (2013). Anthropogenic and natural radiative forcing. In *Climate change 2013: The physical science basis. Contribution of working group I to the fifth assessment report of the intergovernmental panel on climate change* (pp. 659–740). Cambridge University Press. Retrieved from www.climatechange2013.org

Pacific Gas and Electric. (2019). *Energy data request program*. Retrieved from https://pge-energydatarequest.com

Petersen, S. O. (2018). Greenhouse gas emissions from liquid dairy manure: Prediction and mitigation. *Journal of Dairy Science*, *101*(7), 6642–6654. https://doi.org/10.3168/jds.2017-13301

Rodgers, C. D. (2000). *Inverse methods for atmospheric sounding: Theory and practice*. World Scientific.

Safley, L., & Westerman, P. (1988). Biogas production from anaerobic lagoons. *Biological Wastes*, *23*(3), 181–193. https://doi.org/10.1016/0269-7483(88)90033-x

San Joaquin Valley United Air Quality District. (2004). *2004 extreme ozone attainment demonstration plan*. Retrieved from https://www.valleyair.org/Air_Quality_Plans/AQ_Final_Adopted_Ozone2004.htm

Saunois, M., Bousquet, P., Poulter, B., Peregon, A., Ciais, P., Canadell, J. G., et al. (2016). The global methane budget 2000–2012. *Earth System Science Data*, *8*(2), 697–751. https://doi.org/10.5194/essd-8-697-2016

Schwandner, F. M., Gunson, M. R., Miller, C. E., Carn, S. A., Eldering, A., Krings, T., et al. (2017). Spaceborne detection of localized carbon dioxide sources. *Science*, *358*(6360), eaam5782. https://doi.org/10.1126/science.aam5782

Shekhar, A., Chen, J., Paetzold, J. C., Dietrich, F., Zhao, X., Bhattacharjee, S., et al. (2020). Anthropogenic CO_2 emissions assessment of Nile delta using XCO_2 and SIF data from OCO-2 satellite. *Environmental Research Letters*, *15*, 095010. https://doi.org/10.1088/1748-9326/ab9cfe

Skamarock, W. C., Klemp, J. B., Dudhia, J., Gill, D. O., Barker, D., Duda, M. G., et al. (2008). *A Description of the Advanced Research WRF Version 3* (No. NCAR/TN-475+STR). University Corporation for Atmospheric Research. https://doi.org/10.5065/D68S4MVH

Trousdell, J. F., Conley, S. A., Post, A., & Faloona, I. C. (2016). Observing entrainment mixing, photochemical ozone production, and regional methane emissions by aircraft using a simple mixed-layer framework. *Atmospheric Chemistry and Physics*, *16*(24), 15433–15450. https://doi.org/10.5194/acp-16-15433-2016

Turner, A. J., Jacob, D. J., Wecht, K. J., Maasakkers, J. D., Lundgren, E., Andrews, A. E., et al. (2015). Estimating global and North American methane emissions with high spatial resolution using GOSAT satellite data. *Atmospheric Chemistry and Physics*, *15*(12), 7049–7069.

UNEP. (2011). *Near-term climate protection and clean air benefits: Actions for controlling short-lived climate forcers*. United Nations Environment Programme. Retrieved from https://wedocs.unep.org/20.500.11822/8048

VanderZaag, A., Flesch, T., Desjardins, R., Baldé, H., & Wright, T. (2014). Measuring methane emissions from two dairy farms: Seasonal and manure-management effects. *Agricultural and Forest Meteorology*, *194*, 259–267. https://doi.org/10.1016/j.agrformet.2014.02.003

Vaughn, T. L., Bell, C. S., Pickering, C. K., Schwietzke, S., Heath, G. A., Pétron, G., et al. (2018). Temporal variability largely explains top-down/bottom-up difference in methane emission estimates from a natural gas production region. *Proceedings of the National Academy of Sciences of the United States of America*, *115*(46), 11712–11717. https://doi.org/10.1073/pnas.1805687115

Viatte, C., Lauvaux, T., Hedelius, J. K., Parker, H., Chen, J., Jones, T., et al. (2017). Methane emissions from dairies in the Los Angeles Basin. *Atmospheric Chemistry and Physics*, *17*(12), 7509–7528. https://doi.org/10.5194/acp-17-7509-2017

Vogel, F. R., Frey, M., Staufer, J., Hase, F., Broquet, G., Xueref-Remy, I., et al. (2019). XCO_2 in an emission hot-spot region: The COCCON Paris campaign 2015. *Atmospheric Chemistry and Physics*, *19*(5), 3271–3285. https://doi.org/10.5194/acp-19-3271-2019

Wecht, K. J., Jacob, D. J., Frankenberg, C., Jiang, Z., & Blake, D. R. (2014). Mapping of North American methane emissions with high spatial resolution by inversion of SCIAMACHY satellite data. *Journal of Geophysical Research: Atmospheres*, *119*(12), 7741–7756. https://doi.org/10.1002/2014jd021551

Wecht, K. J., Jacob, D. J., Sulprizio, M. P., Santoni, G. W., Wofsy, S. C., Parker, R., et al. (2014). Spatially resolving methane emissions in California: Constraints from the CalNex aircraft campaign and from present (GOSAT, TES) and future (TROPOMI, geostationary) satellite observations. *Atmospheric Chemistry and Physics*, *14*(15), 8173–8184. https://doi.org/10.5194/acp-14-8173-2014

Wood, J. D., Gordon, R. J., & Wagner-Riddle, C. (2013). Biases in discrete CH_4 and N_2O sampling protocols associated with temporal variation of gas fluxes from manure storage systems. *Agricultural and Forest Meteorology*, *171–172*, 295–305. https://doi.org/10.1016/j.agrformet.2012.12.014

Wu, D., Lin, J. C., Fasoli, B., Oda, T., Ye, X., Lauvaux, T., et al. (2018). A Lagrangian approach towards extracting signals of urban CO_2 emissions from satellite observations of atmospheric column CO_2 (XCO_2): X-Stochastic Time-Inverted Lagrangian Transport model ("X-STILT v1"). *Geoscientific Model Development*, *11*(12), 4843–4871. https://doi.org/10.5194/gmd-11-4843-2018

Wu, D., Lin, J. C., Oda, T., & Kort, E. A. (2020). Space-based quantification of per capita CO_2 emissions from cities. *Environmental Research Letters*, *15*(3), 035004. https://doi.org/10.1088/1748-9326/ab68eb

Wunch, D., Jones, D. B. A., Toon, G. C., Deutscher, N. M., Hase, F., Notholt, J., et al. (2019). Emissions of methane in Europe inferred by total column measurements. *Atmospheric Chemistry and Physics*, *19*(6), 3963–3980. https://doi.org/10.5194/acp-19-3963-2019

Wunch, D., Toon, G. C., Sherlock, V., Deutscher, N. M., Liu, C., Feist, D. G., & Wennberg, P. O. (2015). *Documentation for the 2014 TCCON data release*. CaltechDATA. Retrieved from https://data.caltech.edu/records/249

Wunch, D., Wennberg, P. O., Toon, G. C., Keppel-Aleks, G., & Yavin, Y. G. (2009). Emissions of greenhouse gases from a North American megacity. *Geophysical Research Letters*, *36*(15). https://doi.org/10.1029/2009gl039825

Ye, X., Lauvaux, T., Kort, E. A., Oda, T., Feng, S., Lin, J. C., et al. (2020). Constraining fossil fuel CO_2 emissions from urban area using OCO-2 observations of total column CO_2. *Journal of Geophysical Research: Atmospheres*, *125*(8). https://doi.org/10.1029/2019jd030528

Zhang, Y., Gautam, R., Pandey, S., Omara, M., Maasakkers, J. D., Sadavarte, P., et al. (2020). Quantifying methane emissions from the largest oil-producing basin in the United States from space. *Science Advances*, *6*(17), eaaz5120. https://doi.org/10.1126/sciadv.aaz5120

Zhao, X., Marshall, J., Hachinger, S., Gerbig, C., Frey, M., Hase, F., & Chen, J. (2019). Analysis of total column CO_2 and CH_4 measurements in Berlin with WRF-GHG. *Atmospheric Chemistry and Physics*, *19*(17), 11279–11302. https://doi.org/10.5194/acp-19-11279-2019